

# Statistical theory of multiple scattering of waves applied to three-dimensional layered photonic crystals

Alina Ponyavina, Svetlana Kachan, and Nikolaj Sil'vanovich

*Institute of Atomic and Molecular Physics, National Academy of Sciences of Belarus, 70 F. Scorina Avenue, Minsk 220072, Belarus*

Received November 12, 2003; revised manuscript received April 14, 2004; accepted May 5, 2004

On the basis of the statistical theory of multiple scattering of waves, we offer a numerical approach to calculate coherent transmission and reflection for the three-dimensional (3-D) photonic crystals that consist of partially disordered dielectric spheres. With the proposed scheme, which we call the transfer-matrix (TM) method with quasi-crystalline approximation (QCA), we consider a quasi-regular 3-D assembly of particles as a stack of close-packed monolayers with a short-range ordering. Single-scattering characteristics are determined by Mie theory. Lateral electrodynamic coupling between the particles of a monolayer is treated in the QCA. Multibeam interference between monolayers is described in a manner analogous to the TM technique. We apply the TM-QCA calculation technique to study two revealed effects: (1) short-wavelength attenuation due to particles of finite sizes and (2) nonmonotonic dependence of the pseudogap depth on the particle size, refractive-index contrast, and intermonolayer distances. © 2004 Optical Society of America

OCIS codes: 290.4210, 030.1670, 290.5850, 160.4760.

## 1. INTRODUCTION

During the past decade a novel class of optical materials, photonic crystals (PCs), has attracted the attention of many researchers.<sup>1,2</sup> A periodic modulation of the refractive index in such dielectric microstructures leads to a formation of the nontrivial photonic band structure.<sup>3–5</sup> The most dramatic modification of the photonic states in these systems occurs when suitably engineered three-dimensional (3-D) PCs exhibit a frequency range, the so-called complete photonic bandgap (PBG), over which the light propagation is forbidden regardless of the direction of propagation and polarization. However, applications that rely on the Bragg diffraction or strong photonic dispersion in PCs without a complete PBG can also be essentially sufficient to provide a large number of practical needs.

For example, in the late 1980s the pseudogap effect (i.e., formation of frequency ranges in which the photon density of states is strongly suppressed but does not vanish) was used to create new infrared interference-scattering low-pass filters with high steepness.<sup>6</sup> In addition, modification of the spontaneous emission rate of dye solutions impregnating colloidal crystals with a pseudogap has been observed,<sup>7</sup> and distributed-feedback lasing has been realized.<sup>8</sup>

It is clear that any experimental exploration as well as a technological application of PCs has to be accompanied by a quantitative theoretical analysis. Detailed numerical simulations of PC structures allow for the interpretation of experimental data and help to extract the relevant parameters. Perhaps more importantly, the theoretical design of PC structures allows for the identification of the most interesting cases and for the investigation of stable designs for successful operation of devices. During the

past decade there have been many different accurate and approximate theoretical methods developed for these purposes.

Currently the most popular schemes to calculate optical properties of PCs are the plane-wave expansion<sup>9</sup> method, the finite-difference time-domain method,<sup>10</sup> and the transfer-matrix (TM) method.<sup>11</sup> There are also a number of studies based on the theory of multiple scattering of waves that employ an analytical treatment of the diffraction problem on a single scatterer.<sup>5,12–15</sup> These methods allow for the calculation of the band structure as well as the transmission and reflection coefficients of periodic particle arrays.

However, a majority of the applications for PCs requires a defect injection, which gives rise to a disturbance of their perfect periodicity. Of even greater importance is partial topological or size disorder, which is inherent for modern technologies of PC fabrication for the visual and infrared regions. So there are many reasons that such materials are not really perfectly periodic, but are only high-ordered arrays of mesoscopic particles. The most adequate formalism to describe the optical properties of these media, from our point of view, is the approach based on the statistical theory of multiple scattering of waves (STMSW).<sup>16</sup>

The statistical approach to describe 3-D PCs is given in Ref. 17. For example, for the artificial opal the influence of the matrix refractive index and the geometric thickness of a sample on the spectral position and the depth of the transmission dip have been established. Good agreement with the experimental data has been shown. However, to our knowledge the optimization of optical geometric parameters for 3-D opallike PCs has still not been sufficiently explored. In addition, there has been no con-

sideration given to the possibility of controlling the pseudogap properties by a change of interlayer distances or a lateral ordering of monolayers forming 3-D layered PCs.

In this paper we apply the STMSW approach to study the direct transmittance and specular reflectance of 3-D layered PCs such as opals and periodic stacks of close-packed monolayers separated by thin solid films. In Section 2 we provide a detailed description of the applications of the transfer-matrix method with quasi-crystalline approximation (TM-QCA method).

## 2. TRANSFER-MATRIX METHOD WITH QUASI-CRYSTALLINE APPROXIMATION

From the point of view of optics of light-scattering media, formation of PBGs is a result of interference of waves multiply scattered by the ensemble of correlated particles. The higher the space ordering of the disperse medium, the more significant are the collective coherent phenomena such as coherent overirradiation between the particles and interference of waves scattered coherently. There are two main types of high-ordered dispersed layers consisting of spherical particles. They are (i) the structures such as the periodic stack of close-packed monolayers separated by subwavelength thin solid films and (ii) the so-called opallike structures, which consist in the regular array of spheres with a face-centered cubic lattice.

Structure (i) is characterized by at least the one-dimensional regularity leading to the manifestation of the pseudogap that is sensitive not only to the distances between monolayers but also to parameters of individual monolayers<sup>18</sup> (Fig. 1). Structure (ii) is ordered in all three dimensions similar to a mesoscopic crystalline lattice. This is an example of a 3-D PC that can be regarded as the special case of (i) with the regular monolayers and intermonolayer distances equal to the particle size.

The STMSW operates with the field moments, which are the values averaged over the statistical ensemble of particles. It means that all possible configurations of the given particle array are taken into account. The main field characteristics of the STMSW are the first and second moments, i.e., the average (or coherent) field  $\langle \mathbf{E}(\mathbf{r}) \rangle$  and the field covariation  $\langle \mathbf{E}(\mathbf{r}) \cdot \mathbf{E}^*(\mathbf{r}) \rangle$ .

The coherent field  $\langle \mathbf{E}(\mathbf{r}) \rangle$  is determined from the following chain of equations:

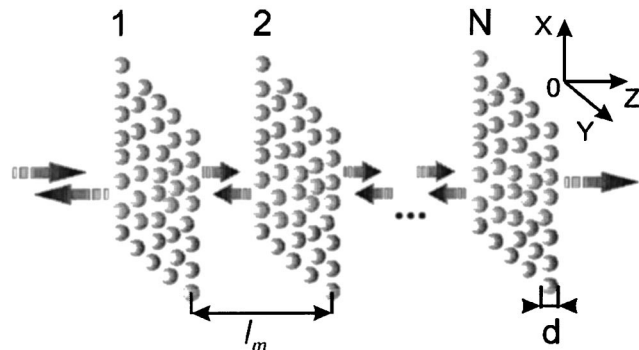


Fig. 1. Scheme of light interaction with the stratified system of particle monolayers.

$$\langle \mathbf{E}(\mathbf{r}) \rangle = \mathbf{E}_0 + p_0 \int \mathbf{t}(\mathbf{r}, \mathbf{r}_i) \langle \mathbf{E}(\mathbf{r}_i) \rangle_i d\mathbf{r}_i, \quad (1)$$

$$\begin{aligned} \langle \mathbf{E}(\mathbf{r}_i) \rangle_i &= \mathbf{E}_0 + p_0 \int g(\mathbf{r}_i, \mathbf{r}_j) \mathbf{t}(\mathbf{r}_i, \mathbf{r}_j) \\ &\quad \times \langle \mathbf{E}(\mathbf{r}_j) \rangle_j d\mathbf{r}_j, \end{aligned} \quad (2)$$

and so on. Here  $\langle \mathbf{E}(\mathbf{r}) \rangle$  is the field averaged over all configurations of particles;  $\langle \mathbf{E}(\mathbf{r}_i) \rangle_i$  is the averaged field with one fixed particle;  $\langle \mathbf{E}(\mathbf{r}_i) \rangle_{ij}$  is the averaged field with two fixed particles;  $p_0$  is the average concentration of particles;  $g(\mathbf{r}_i, \mathbf{r}_j)$  is the binary correlation function, which determines the probability of the location of the centers of two particles at points  $\mathbf{r}_i$  and  $\mathbf{r}_j$ , correspondingly.

Some special procedures were developed to interrupt the chains of equations and determine the coherent field and coherent intensity  $I_c = |\langle \mathbf{E}(\mathbf{r}) \rangle|^2$ . The most well-known calculation schemes of the STMSW are the single-scattering approximation, the effective field approximation, and the quasi-crystalline approximation (QCA). They differ from each other in the manner of the effective field description.

The QCA seems to be the most advanced technique. The main assumption of the QCA, proposed by Lax,<sup>19</sup> is that  $\langle \mathbf{E}(\mathbf{r}) \rangle_{ij} \approx \langle \mathbf{E}(\mathbf{r}) \rangle_i$ . This approximation supposes that fixation of any particle specifies the spatial configuration of the whole assembly. For a random monolayer, the closer the structure is to the crystalline assembly, the more justifiable is this assumption.

The stratified and opallike structures can be considered as layer periodic dispersed structures. In our opinion, the most natural scheme of their optical characterization is based on the solution of the problem in two steps: (i) determination of the vector scattering amplitude of a monolayer and then (ii) consideration of the electromagnetic interactions between all monolayers of the sample through a self-consistent procedure such as the well-known *T*-matrix technique.<sup>11</sup>

The most principal step is the first stage that is applied to the lateral electrodynamic coupling of particles in a high-ordered monolayer. For this first stage, we propose using the STMSW approach, especially the well-developed<sup>20</sup> QCA.

In Subsections 2.A and 2.B we briefly consider the fundamental points of the TM-QCA method used in this paper to study the pseudogap properties of 3-D PCs containing mesoscopic spherical dielectric particles.

### A. Vector Scattering Amplitude of a Close-Packed Monolayer

Let us consider an infinite monolayer lying along the *X*, *O*, *Y* plane and irradiated by a plane-polarized wave coming along the *z* direction. Then by use of the Green function approach, the ensemble-averaged field  $\langle \mathbf{E}(\mathbf{r}) \rangle$  and the effective field inside a particle  $\langle \mathbf{E}(\mathbf{r} + \mathbf{R}) \rangle_R$  are described in the QCA by the following system of equations:

$$\langle \mathbf{E}(\mathbf{r}) \rangle = \mathbf{e} \exp(ikz) + \frac{2\pi i}{k} p_0 \mathbf{f}(\pm \mathbf{z}) \exp(ikz),$$

$$\begin{aligned}
\langle \mathbf{E}(\mathbf{r} + \mathbf{R}) \rangle_R &= \mathbf{e} \exp(ikz) + \int d\mathbf{r} \vec{\Gamma}(\mathbf{r} + \mathbf{R}, \mathbf{r}' + \mathbf{R}) \\
&\times \langle \mathbf{E}(\mathbf{r}' + \mathbf{R}) \rangle_R + p_0 \int d\mathbf{R}' g(|\mathbf{R} - \mathbf{R}'|) \\
&\times \int d\mathbf{r}' \vec{\Gamma}(\mathbf{r} + \mathbf{R}, \mathbf{r}' + \mathbf{R}') \\
&\times \langle \mathbf{E}(\mathbf{r}' + \mathbf{R}') \rangle_{R'}, \quad (3)
\end{aligned}$$

where

$$\mathbf{f}(\pm \mathbf{z}) = \frac{k^2}{4\pi} (\bar{n}^2 - 1) \int_V d\mathbf{r}' \exp(\pm ikz) (\vec{\Gamma} - \mathbf{z}\mathbf{z}) \langle \mathbf{E}(\mathbf{r}') \rangle \quad (4)$$

is the vector scattering amplitude of a single particle;  $p_0$  is the surface concentration of particles;  $\vec{\Gamma}(\mathbf{r}, \mathbf{r}')$  is the tensor Green function; and  $k$  is the wave number. The space integral of Eq. (4) is taken over a particle's volume. The plus and minus signs correspond to the transmitted and reflected waves, respectively;  $\mathbf{z}$  is a unit vector along the  $z$  axis.

According to Eqs. (3), we can introduce the vector scattering amplitude of a monolayer:

$$\mathbf{F}(\pm \mathbf{z}) = \frac{2\pi i}{k} p_0 \mathbf{f}(\pm \mathbf{z}). \quad (5)$$

The monolayer scattering amplitude  $\mathbf{F}(\pm \mathbf{z})$  is expressed in terms of the vector scattering amplitude of a single particle  $\mathbf{f}(\pm \mathbf{z})$ , which is determined with the over-irradiation between the particles taken into account. When a monolayer comprises particles of a spherical shape, one can solve Eqs. (3) by expanding all fields, even the incident one, into the vector spherical functions and then determine the corresponding coefficients from a set of linear algebraic equations.<sup>18,20</sup> Then the expression for the single-scattering amplitude takes the form

$$\mathbf{f}(\pm \mathbf{z}) = \mathbf{e} \frac{i}{2k} \sum_{l=1}^{\infty} (\pm 1)^l (2l + 1) (\beta_l \pm \alpha_l).$$

Use of the additional theorem for the vector spherical functions when we integrate Eqs. (3) for the unknown coefficients  $\beta_l$  and  $\alpha_l$  yields the following system of the equations:

$$\beta_l = b_l + p_0 b_l \sum_l (P_l \beta_l + Q_l \alpha_l),$$

$$\alpha_l = a_l + p_0 a_l \sum_l (P_l \alpha_l + Q_l \beta_l).$$

Here  $a_l$  and  $b_l$  are the Mie coefficients; functions  $P_l$  and  $Q_l$  are expressed in a complicated manner<sup>18,20</sup> through the Legendre polynomials and the characteristic functions  $H_p = 2\pi \int_0^\infty dR R g(R) h_p^{(1)}(kR)$ , where  $h_p^{(1)}$  is the Hankel function. Calculation of the radial distribution function for the dense particle monolayer is carried out in the Percus–Yevick approximation for solid spheres<sup>21</sup> when the degree of particle ordering and the subsequent features of the radial distribution function are determined by the overlap parameter  $\eta = p_0 \pi d^2/4$ . Numeri-

cal simulation of  $g(r)$ ,  $\beta_l$ , and  $\alpha_l$  is performed with the iteration method. As the Mie coefficients are determined, we employ the reverse recursion technique.

## B. Multilayer Scattering System

To calculate the coefficients of coherent transmission and reflection of a multilayer scattering system we use the technique described in this subsection.

Let the distances between the neighboring parallel monolayers be equal and the propagation vector of the incident plane wave be transverse to the monolayer surfaces and parallel to the  $\mathbf{z}$  unit vector. To describe the coherent field of a single monolayer we apply the expressions obtained by the QCA for the vector scattering amplitudes  $\mathbf{F}^\pm = \mathbf{F}(\pm \mathbf{z})$  [see Eqs. (3)–(5)]. Then the coherent field of the whole sample consisting of  $N$  monolayers can be determined as

$$\begin{aligned}
\langle \mathbf{E}(\mathbf{z}) \rangle &= \exp(ikz) \left( \mathbf{e} + \sum_{j=1}^N \mathbf{G}_j^+ \right), \\
\langle \mathbf{E}(-\mathbf{z}) \rangle &= \exp(ikz) \left\{ \sum_{j=1}^N \mathbf{G}_j^- \exp[(j - 1)2ikl_m] \right\}. \quad (6)
\end{aligned}$$

Here  $\mathbf{G}_j^\pm = \mathbf{G}(\pm \mathbf{z})$  are the scattering amplitudes in the forward and backward directions for the  $j$ th monolayer in the presence of the other monolayers of the system;  $l_m$  is the interlayer distance, i.e., the spatial interval between the centers of neighboring monolayers (see Fig. 1).

The method of a self-consistent field, which allows us to consider electrodynamic interactions between the layers, is an effective technique to find  $\mathbf{G}_j^\pm$ . It yields the following system of equations:

$$\begin{aligned}
\mathbf{G}_j^+ &= \mathbf{F}^+ + \mathbf{F}^+ \sum_{p=1}^{j-1} \mathbf{G}_p^+ + \mathbf{F}^- \sum_{p=j+1}^N \mathbf{G}_p^- \\
&\times \exp[(p - j)2ikl_m], \\
\mathbf{G}_j^- &= \mathbf{F}^- + \mathbf{F}^- \sum_{p=1}^{j-1} \mathbf{G}_p^+ + \mathbf{F}^+ \sum_{p=j+1}^N \mathbf{G}_p^- \\
&\times \exp[(p - j)2ikl_m]. \quad (7)
\end{aligned}$$

The sums in these expressions take into account the coherent irradiation of the  $j$ th monolayer by the other monolayers. Solving the set relative to  $\mathbf{G}_j^\pm$  and putting it in Eqs. (6), one can find the coherent field of the multilayer structure composed of equidistant monodisperse layers. However, this technique is also effective for the case of polydisperse monolayers<sup>18</sup> as well as for monolayers separated by films distinguished by thickness.

At this second stage the method proposed is close to the TM approach with only the monolayer amplitude function determined in the QCA of the STMSW. That is why we refer to the scheme as the TM-QCA method.

Note that at a plane-wave incident on the plane-parallel dispersed layer, spectral coefficients of coherent transmission and reflection can be defined through the co-

herent field as  $T = |\langle \mathbf{E}(\mathbf{z}) \rangle|^2$  and  $R = |\langle \mathbf{E}(-\mathbf{z}) \rangle|^2$ , respectively. It is worthwhile to remember that coherent  $T$  and  $R$  correspond to the coefficients of direct transmission and specular reflection measured in the case of the small angular detection.

### 3. RESULTS AND DISCUSSION

In this section we use the TM-QCA calculation scheme to study the dependence of pseudogap characteristics of 3-D layered PCs on the refractive-index contrast, particle mean size, and intermonolayer distances. We focus on the nature of the enhanced attenuation over the blue range off a pseudogap and analyze the revealed nonmonotonic dependence of this transmission interference dip on the named parameters. To separate the role of system ordering in the third direction (stacking), we also consider spectral dependences of monolayer transmittance and reflectance.

#### A. Photonic Crystal Transmission Spectra Characterization

A typical transmission spectrum of a 3-D layer-periodic assembly of mesoscopic spheres is presented in Fig. 2. As one can see, the main feature is the presence of a transmission dip over the range of wavelengths comparable with particle sizes. It is caused by the suppression of wave propagation due to the spatial ordering of mesoscopic particles. In addition, there is a strong attenuation of transmission in the high-frequency region. This effect is in agreement with numerous experimental data (see, for example, Refs. 17 and 22–24), and its nature is discussed in Subsection 3.B.

To characterize the transmission spectra quantitatively, let us introduce the following parameters (see Fig. 2): the spectral position ( $\lambda_0$ ), the residual transmittance ( $T_0$ ), and the bandwidth ( $\Delta_\omega$ ) of the PBG (or pseudogap), as well as short-wavelength attenuation characteristics—transmittances in the high-frequency ( $T_<$ ) and low-frequency ( $T_>$ ) gap edges and the width ( $\Delta_<$ ) of the high-frequency transmission range (i.e., transmission band, high-frequency relative to the first PBG).

The principal characteristic of a PC is the spectral position  $\lambda_0$  of the PBG. Experimental data<sup>17</sup> show the

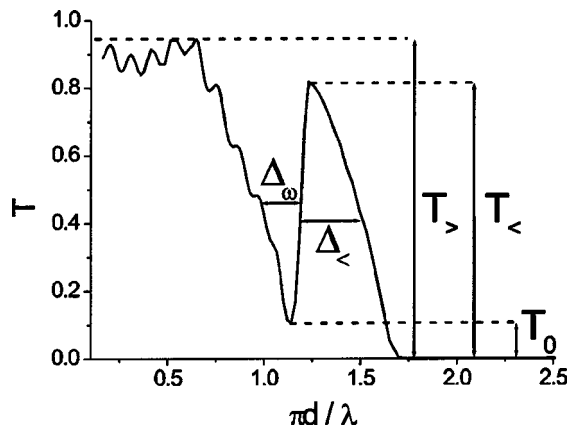


Fig. 2. Coherent transmission spectra of the multilayer system of dielectric spheres ( $N = 8$ ,  $\eta = 0.6$ ,  $\bar{n} = 1.26$ ,  $l_m = 1.23d$ ).

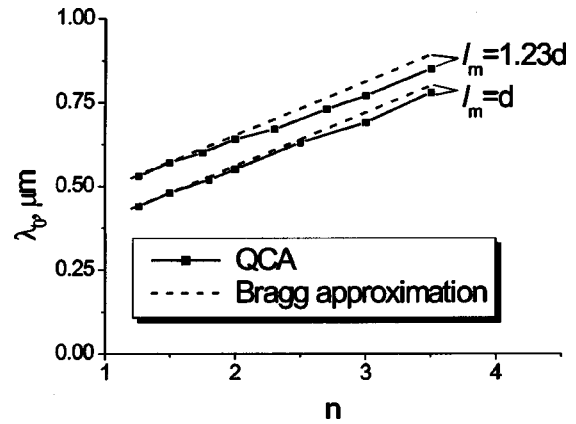


Fig. 3. Dependence of the pseudogap spectral position  $\lambda_0$  on the refractive-index contrast for the multilayer system of close-packed dielectric spheres with the different interlayer distances  $l_m$ . Calculations were performed by the QCA and the Bragg approximation ( $N = 8$ ,  $\eta = 0.6$ ,  $d = 200$  nm).

monotonic increase of  $\lambda_0$  when the particle refractive index grows. As can be seen from the solid curves in Fig. 3, our calculations confirm this dependence.

The main tendencies of the dependence of  $\lambda_0$  on optical and geometric parameters of the 3-D layered PCs can be concisely described by the simple analytical expression derived from the analog of the Bragg conditions for a PC. From the Bragg approximation for the interference minimum in forward direction  $n_{\text{eff}} l_m = \lambda_0/2$ , one can obtain the simple expression connecting the gap position, particle and matrix refractive indices, particle sizes, and filling fraction in a PC:

$$\lambda_0 \approx 2l_m [cn_p + (1 - c)n_m]. \quad (8)$$

Here we define the effective refractive index of the PC  $n_{\text{eff}}$  as a sum of the refractive indices of particles  $n_p$  and matrix  $n_m$  in regard to the particle filling fraction  $c$ :  $n_{\text{eff}} = cn_p + (1 - c)n_m$ . As one can see by approximation (8), the increase of intermonolayer distances or the particle refractive index gives rise to the long-wavelength shift of the bandgap. Note that for opals or inverse opals the interfacial spacing  $l_m$  is equal to the mean particle size  $d$ . Thus  $\lambda_0 \approx 2d[cn_p + (1 - c)n_m]$  (see, for example, Ref. 25).

The quantitative agreement between the TM-QCA and the Bragg approximation calculations is illustrated in Fig. 3. In our opinion, this good agreement is the consequence of the fact that the above-described modeling of the 3-D PC as a stack of monolayers is in some relation close to the classical treatment of x-ray Bragg diffraction into a crystal. Both the TM-QCA and the Bragg approximation consider an interference of waves scattered by crystal planes.

However, the TM-QCA method also solves two problems of great importance for wave propagations in a spatially ordered system of strong scatterers (such as particles with a relative refractive index  $\bar{n} > 1.5$ ). For the first, the TM-QCA method involves the rigorous solution of a diffraction problem on a single sphere (the Mie theory) that allows us to describe light interaction with the nonpoint scatterers. Second, we take into account electrodynamic coupling between the particles in a planar

monolayer. Both of these topical points are extremely important for a description of the full set of PC characteristics mentioned at the beginning of this subsection.

### B. High-Frequency Attenuation in Direct Transmittance

The PC spectral coefficients of coherent transmission and reflection calculated over the range from 100 to 1400 nm for different particle sizes are presented in Fig. 4. The reservation of the spectral position of the first pseudogap was achieved by the appropriate choice of interlayer distances [see approximation (8)].

As one can see, for small particles there is a set of secondary gaps in the short-wavelength range relative to the pseudogap position. In general, the dependence of the pseudogap depth on its order is nonmonotonic (see, for example, the transmission spectrum for  $d = 100$  nm). In addition, a comparison of the data in Fig. 4(a) also shows the nonmonotonic dependence of the first pseudogap depth on particle size. The common cause underlying these effects is discussed in detail in Subsection 3.D.

However, the other feature is more interesting. When the particle size increases and becomes comparable to the stack period  $l_m$  (and consequently to the wavelength of the first pseudogap), the attenuation in the short-wavelength region grows. It leads to a decreasing width ( $\Delta_{<}$ ) of the high-frequency transmission range. The usual explanation of experimental evidence of this effect is imperfect ordering in real PCs, which produces multiple incoherent (so-called diffuse) scattering and so diminishes the transport mean free path.<sup>26</sup> But we should emphasize that, in the given case, the degree of spatial

disordering of samples with different sizes was the same because of the same monolayer overlap parameter. That is why we can conclude that this additional short-wavelength attenuation for samples containing large particles can be connected with the spectral features of single light scattering.

It is well known that the cross section of single scattering grows with an increase of the size parameter  $\rho = \pi d/\lambda$ . Attenuation of radiation connected with its scattering on a single particle becomes stronger as the frequency increases.<sup>27</sup> Correspondingly, the high-frequency barrier appears in the direct transmission spectra of disperse media with any type of arrangement (even for the perfect spatial array). The larger the particle sizes, the longer the wavelength in this transmission barrier. For 3-D layered PCs the particle enlargement at fixed  $l_m$  makes the blue transmission cutoff closer to the first pseudogap position. In addition, the cutoff steepness factor rises at the higher particle refractive index. So the growth of the particle relative refractive index results in the narrowing high-frequency transmission range  $\Delta_{<}$ . Because the efficiency of a PC depends on both the bandgap depth and the width of the transmission bands beyond it, an increase in  $\bar{n}$  is advisable only up to some value determined by practical necessity. Also, to observe the pronounced bandgap in the structures with the high refractive-index contrast, it is necessary to meet the severe demand for packing quality and particle monodispersity.

The effect of coherence loss for scattered waves due to the particle size comparability with the wavelength is of

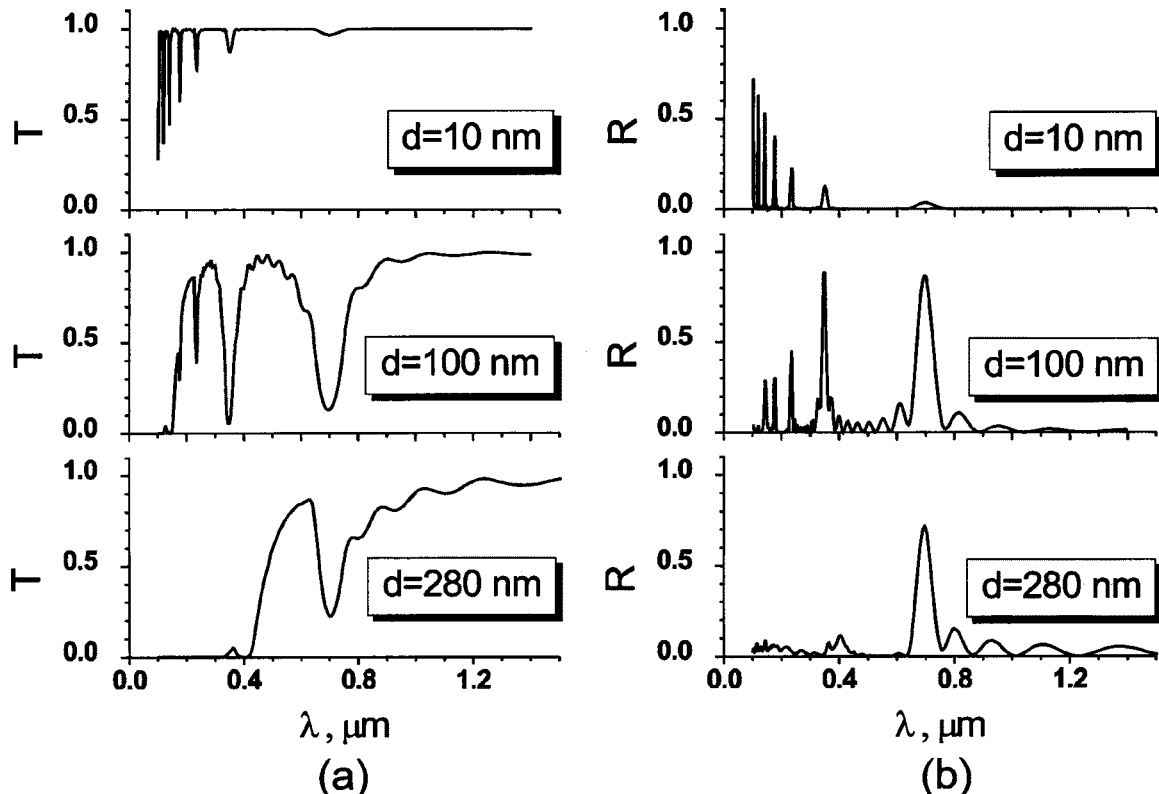


Fig. 4. (a) Coherent transmission and (b) specular reflection spectra of the multilayer systems of close-packed monolayers with different particle sizes ( $N = 8$ ,  $\eta = 0.6$ ,  $\bar{n} = 1.6$ ). All multilayer systems are stacked so that the pseudogap positions are coincident (for  $d = 10$  nm,  $l_m = 347.6$  nm; for  $d = 100$  nm,  $l_m = 326$  nm; for  $d = 280$  nm,  $l_m \approx d$ ).

principal importance, and not just for the treatment of high-frequency attenuation in direct transmittance. From the same point of view we can provide answers to the problem as to why it is so difficult to experimentally create the complete bandgap and absolute transparency of a PC in the spectral ranges out of the bandgap. There is an additional physical reason other than such evident reasons as size disorder of particles and destruction of the PC's periodicity. This additional reason is the loss of coherence and energy dissipation due to the finite sizes of the particles.

As was mentioned above, every particle in a PC can be considered as the source of scattered waves, and a bandgap results because of the interference summing of these scattered waves. It seems apparent that a decrease in the degree of the mutual coherence of scattered waves will change the interference pattern. It is common knowledge that the finite size of the light source gives rise to a decrease in the spatial coherence of waves. In its turn, this circumstance leads to the degradation of the contrast of the interference pattern created by two or more sources of a finite size. From the above reasoning, in our opinion, an interference destruction of the bandgap may be the result not only of some spatial disordering of real photonic structures, but also of such fundamental causes as the particle finite (compared with wavelength and interparticle distances) size.

### C. Collective Attenuation Resonance in a Dense Monolayer and Efficiency of the Interlayer Interference

To clarify the possible mechanisms initiating the formation of PBGs, let us consider a simplified situation in which the layered structure includes only two monolayers of close-packed spherical particles (see Fig. 5). In this case the main contribution in the interference sum is provided by the light rays passing through both monolayers with no reflection (1) and by the light rays experiencing twofold reflection (2).

To possess the efficient interference, the intensities (amplitudes) of light rays of these two types should be significantly large. That is, the transmission coefficient  $T_m$

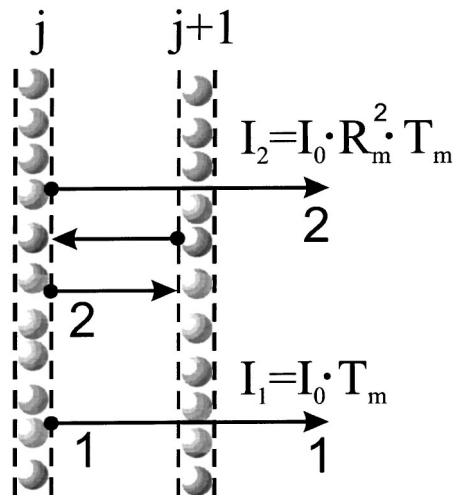


Fig. 5. Interference scheme for light rays passing through neighboring monolayers with no reflection (1) and experiencing twofold reflection (2).

of one monolayer should have a high value. Also, both intensities should be comparable:  $I_1 \approx I_2$ . The latter condition is satisfied when  $T_m(1 - R_m^2)$  vanishes. Thus, combining the conditions of large  $T_m$  and small  $T_m(1 - R_m^2)$ , we conclude that the monolayer reflection coefficient  $R_m$  should also be significant. Let us introduce the function  $f = 1 - T_m(1 - R_m^2)$ , which we refer to as the function of the efficiency of interlayer interference. We can say that the deepest pseudogap is reached at maximal  $f$  while  $T_m$  and  $R_m$  are kept relatively large.

To establish the range of parameters for which these conditions are satisfied simultaneously, let us consider the spectral dependence of transmission and reflection coefficients for the close-packed monolayer. Figure 6 shows  $T_m$ ,  $R_m$ , and  $f$  as functions of the size parameter  $\rho$  for three values of the refractive-index contrast  $\bar{n}$  (1.26, 2.0, 3.5). The overlap parameter in all cases is unchanged and is equal to  $\eta = 0.6$ . The dashed curves in the middle panels of Fig. 6 show the transmission spectra for sparse systems equivalent to monolayers with an appropriate number and type of particles.

As the lower panels of Fig. 6 illustrate, there are two maxima of  $R_m$  over the size-parameter range under consideration. From a comparison of the middle and lower panels, it can be seen that, in the region of the second (short-wavelength) resonance of reflection, the  $T_m$  value is decreasing because of the strong single scattering (i.e., the Mie resonance). Apparently (see the upper panels of Fig. 6) it prevents the efficient interlayer interference of light in the corresponding frequency range. At the same time, the above-formulated conditions of the efficient interference are obviously satisfied over the range of the first (long-wavelength)  $R_m$  resonance, for which the transmission coefficient remains large. Note that when the refractive index of particles increases, this optimal range shifts to the smaller size parameter's values. For  $\bar{n} = 1.26, 2.0, \text{ and } 3.5$  we obtain, respectively,  $\rho \approx 1, 0.7, \text{ and } 0.5$ .

Note that the first maximum in the reflection spectrum as well as the coincident minimum in transmission of a monolayer have a fundamentally collective nature. This collective nature is proved by the absence of the appropriate dip in transmission spectra of the sparse system (see the middle panels in Fig. 6). Most likely the additional transmission attenuation, which arises in this spectral region for the close-packed systems, is related to the short-range ordering of particles, resulting in strong lateral electrodynamic couplings on the scales of the particles' correlation. Qualitatively, the origin of this resonance attenuation can be associated with some effective scatterers (agglomerates) of the size larger than the size of a single particle, which emerge in the close-packed monolayer. The larger the overlap parameter of the partially ordered monolayer, the higher the probability of formation for such agglomerates. The growth of the refractive index of particles leads to the enhanced lateral electrodynamic coupling, which manifests in increasing the corresponding collective attenuation [compare the middle panels of Figs. 6(a)–6(c)].

The considered collective attenuation resonance in the region  $\rho < 1$  has already been revealed both in experimental and in numerical data.<sup>20</sup> Its emergence and col-

lective nature are indirectly demonstrated by the detection of reflection resonance for a close-packed monolayer<sup>28</sup> and concentrative transformation of the angular distribution of radiation scattered by it over the certain spectral range.<sup>29</sup>

Thus, in our opinion, the first (long-wavelength) resonance attenuation of the close-packed monolayer is essentially collective in itself and is determined by the lateral electrodynamic coupling of near-ordered scatterers.

In its turn, the second (short-wavelength) resonance of reflection as well as the coincident minimum in transmission of a monolayer is principally related to the light scattering on single spherical particles. This Mie resonance is exhibited both in a sparse random system of noninteracting particles and in a close-packed two-dimensional layer. Some distinction in these appearances arises because of the above-discussed concentration effect based on

coherent electrodynamic coupling of spatially correlated particles in a monolayer. It consists in the formation of the effective field inside the layer, which is essentially different from the incident field. Namely, this change in the field interacting with a particle gives rise to some spectral shift and modification of the Mie-scattering resonance band when a sparse system turns into the close-packed monolayer (see Fig. 6, middle panels).

In Fig. 7(a) we present the transmission spectra of PCs and of the corresponding sparse system of random distributed particles. One can clearly see from the comparison of these spectra that a feature of the PC spectrum is the existence of a narrow and deep attenuation band in the vicinity of  $\rho \approx 0.8$ . It is just the band, which is absent in transmission spectra of a sparse random system. It has a coherent nature and is determined by interlayer interference. In contrast, the deep gap in the region, which is

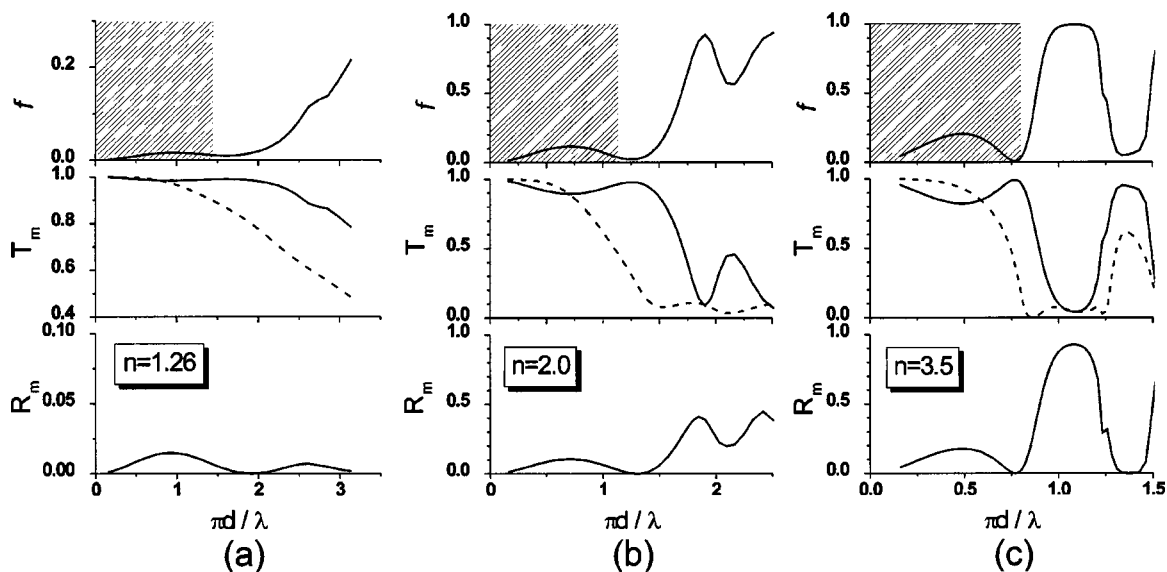


Fig. 6. Spectral dependence of coherent transmission  $T_m$ , specular reflection  $R_m$ , and the function of the efficiency of interlayer interference  $f = 1 - T_m(1 - R_m^2)$  at light interacting with the close-packed ( $\eta = 0.6$ ) monolayers of spherical particles ( $d = 200$  nm) with different  $\bar{n}$ . The dashed curves correspond to transmission coefficients for the sparse systems of the same number and type of scatterers.

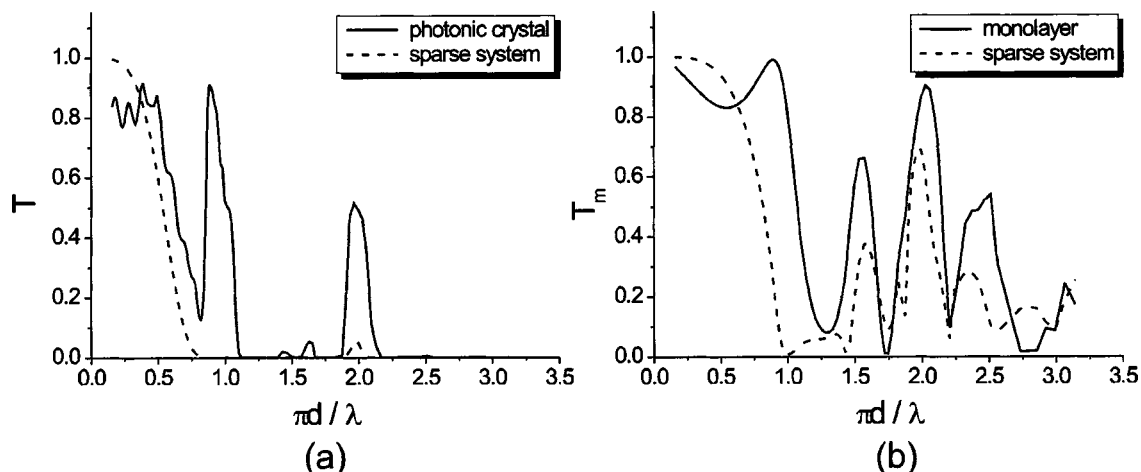


Fig. 7. Coherent transmission spectra of (a) the multilayer ( $N = 8$ ,  $l_m = 1.23d$ ) and (b) the monolayer structures of dielectric spherical particles ( $d = 200$  nm,  $\eta = 0.6$ ,  $\bar{n} = 3.0$ ). The dashed curves correspond to the sparse systems of the same number and type of scatterers.

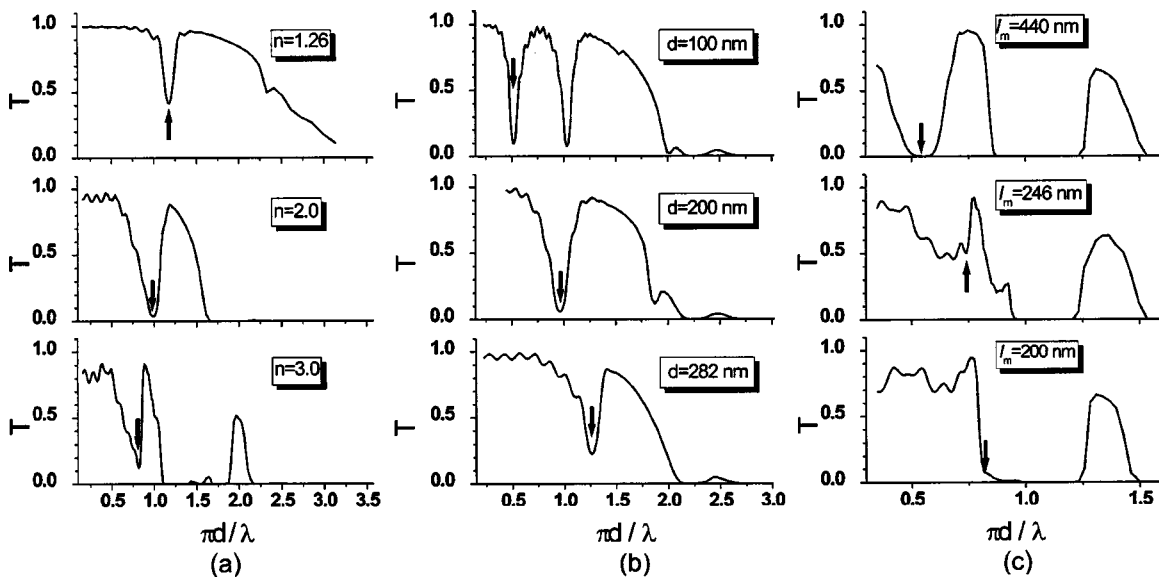


Fig. 8. Dependence of coherent transmission spectra of the multilayer system ( $N = 8$ ,  $\eta = 0.6$ ) of dielectric spheres (a) on the refractive-index contrast ( $d = 200$  nm,  $l_m = 1.23d$ ); (b) on the particle diameter ( $\bar{n} = 1.6$ ,  $l_m = 282$  nm); (c) on the interlayer distance ( $d = 200$  nm,  $\bar{n} = 3.5$ ). Arrows indicate the pseudogap spectral position.

present in the spectra of both systems, is related to the strong resonances of single scattering. It is not caused by the periodicity of the refractive index, which is crucial for PCs.

This conclusion is also supported by the data presented in Fig. 7(b), which show the transmission spectra of both the monolayer of close-packed particles and the sparse system with the corresponding number of particles. It is evident that the transmission spectra of the monolayer and sparse random system have the same fine structure features over the Mie resonance region ( $\rho > 1.1$ ).

#### D. Dependence of Pseudogap Depth on Optical and Structural Parameters of Three-Dimensional Layered Photonic Crystals

As we mentioned in the discussion of the results presented in Fig. 4, the spectral position of the pseudogap in the structures under consideration can be tailored by a change in the particles' size or interlayer distance. In Fig. 6 this region is hatched. The right demarcation line of the hatched region corresponds to the minimal (from all the possible) value of interlayer distance  $l_m = d$ . Increasing the ratio  $l_m/d$  (for example, by decreasing  $d$ ) leads to the shift of the pseudogap to the range of lower values of the size parameter. In this case the function of the efficiency of interlayer interference  $f$  is changed nonmonotonically (see the upper panels in Fig. 6). It first increases with decreasing  $d$  to some critical value  $d_0$ , but then starts to diminish. Also, as one can see from Fig. 6, the larger the refractive index of the particles, the larger the maximal value of the function  $f$ , and accordingly better optimal conditions for the pseudogap opening can be reached. Such behavior of function  $f$  is connected with the collective attenuation resonance in a monolayer with short-range ordering.

Thus the existence of the additional collective attenuation band, which is sensitive to such parameters of the monolayer as the refractive index, size, and packing den-

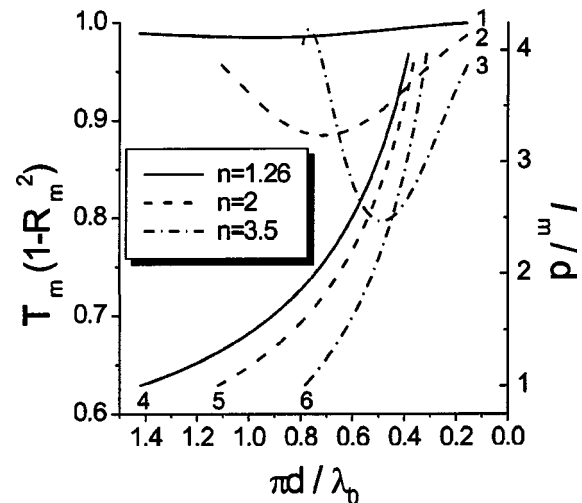


Fig. 9. Dependence of the function  $T_m(1 - R_m^2)$  (curves 1–3) and the relative interlayer distance  $l_m/d$  (curves 4–6) on the pseudogap spectral position for the multilayer systems of close-packed ( $\eta = 0.6$ ) monolayers with different  $\bar{n}$ .

sity of particles, can cause the nonmonotonic dependence of the pseudogap depth on several parameters of the PC. Such consideration provides a qualitative explanation of the nonmonotonic dependence of the pseudogap depth, presented in Fig. 4, on the particles' size for the 3-D layered PC structures with  $\lambda_0 = \text{const}$ . The same explanation can also be provided for the results, presented in Fig. 8, which demonstrate nonmonotonic dependence of the pseudogap depth on (a) the refractive-index contrast, (b) the particles' size (in the case of structures with  $l_m = \text{const}$ ), and (c) the interlayer distances.

A deeper insight into these effects is presented in Fig. 9. We start with the consideration of the pseudogap depth on the refractive-index contrast. As one can see, when the refractive index increases, the minimum of the function  $T_m(1 - R_m^2)$  (see curves 1–3) shifts to the lower

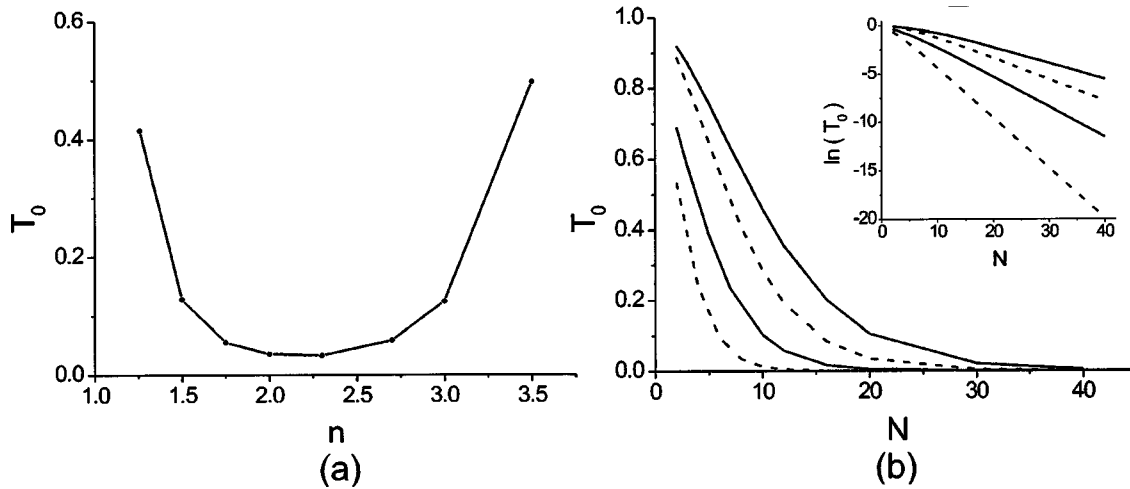


Fig. 10. Dependence of the residual transmittance  $T_0$  (a) on the refractive-index contrast ( $N = 8$ ,  $d = 200$  nm,  $\eta = 0.6$ ,  $l_m = 1.23d$ ) and (b) on the number of layers in the multilayer system [ $d = 200$  nm,  $\eta = 0.6$ ,  $l_m = d$  (solid curves),  $l_m = 1.23d$  (dashed curves)]. The two upper curves correspond to  $\bar{n} = 1.26$  and the two lower curves correspond to  $\bar{n} = 2$ . The inset shows the logarithm of the residual transmittance  $T_0$  by the number of layers.

values of the size parameter  $\rho$ . For the analyzed range of the refractive indices, the pseudogap depth increases monotonically with increasing  $\bar{n}$  only for  $\rho < 0.65$ . In contrast, as illustrated by spectra presented in Fig. 8(a), for  $\rho > 0.65$  this dependence becomes nonmonotonic.

The origin of the nonmonotonic dependence of the pseudogap depth on particle size  $d$  was discussed above when we considered Fig. 4. In Fig. 8(b) we plot another dependence, now keeping  $l_m/d$  constant. As we can see, in this case the change in particle size results in the shift of its spectral position (together with the nonmonotonic dependence of the depth of the interference dip).

Interpretation of the data presented in Fig. 8(c) is more complicated. Here we can see that for a PC with  $\bar{n} = 3.5$  the pseudogap depth at first decreases and then grows as  $l_m$  varies from 440 to 200 nm. Referring to Fig. 9 (see curves 3 and 6), we note in this case that the values of the size parameter, corresponding to the pseudogap, are 0.55, 0.74, and 0.82 whereas  $l_m/d$  changes from 2.2 to 1. This range of  $\rho$  corresponds to a nonmonotonic change of the function of efficiency of interlayer interference, but its values at  $\rho = 0.82$  and 0.74 are equal ( $f = 0.98$ ) and one can expect the equivalent pseudogap depths. However, it can be concluded from Figs. 6 and 9 that the value  $\rho = 0.82$  is close to the transition region from the collective attenuation band to the strong resonance of single scattering. As one can see from Fig. 8(c), in this case the narrow pseudogap is absorbed by the broad band of strong single attenuation (see the spectrum for  $l_m = 200$  nm). Thus, as we discussed in Subsection 3.C, this broad attenuation band is essentially the result of the Mie resonance scattering and does not reflect the interferential nature of PBGs.

In Fig. 9 we also illustrate how the parameters  $d$  and  $l_m$  can be optimized to reach the maximal pseudogap depth for some given values of the refractive-index contrast and  $\lambda_0$ . Let us demonstrate this action by the example of particles with the relative refractive index equal to 3.5. Fixing the required wavelength  $\lambda_0$ , one can determine  $d$  from the size parameter value  $\rho = 0.49$ , which

corresponds to the minimum of curve 3. Farther, when we specify from curve 6 the value of  $l_m/d = 2.2$ , appropriate to  $\rho = 0.49$ , it is easy to define the interlayer spacing  $l_m$ .

As Fig. 9 shows, the optimal ratio of  $l_m/d$  is close to unity only for small values of the refractive index, and thus the opallike structures (for which  $l_m = d$ ) become optimal. However, when the refractive index of the particles increases, the maximal pseudogap depth is reached at  $l_m$ , which is large compared with  $d$ .

Figures 10(a) and 10(b) depict the dependence of the residual transmission in the pseudogap range on the refractive index of particles and on the number of layers, respectively. As one can see from Fig. 10(a), the optimal values of the refractive index lie in the region  $\bar{n} = 1.75$ – $2.75$ . However, it should be emphasized that the higher the refractive index or the ratio  $l_m/d$ , the smaller the number of layers required to reach the asymptotic value of the residual transmission and to achieve the asymptotic linear dependence of  $\ln(T_0)$  by  $N$ , experimentally detected for artificial opals<sup>24</sup> [see Fig. 10(b)].

It should be noted that in all the presented estimations we assumed the constant overlap parameter. Its change causes a transformation of the monolayer spectrum and, as a consequence, changes the optimal values of the structure parameters.

#### 4. CONCLUSIONS

We have studied 3-D layer periodic dispersed arrays of spherical particles applying the TM-QCA method and have revealed several qualitative features of their optical transmittance spectra. The main feature consists in the nonmonotonic dependence of the pseudogap depth on such parameters as particle size, refractive-index contrast, and intermonolayer distance. The origin of this effect lies in the existence of the limited spectral range where the lateral electrodynamic coupling in a single close-packed monolayer of spherical particles is maxi-

mized. As a consequence, the coherent reflectance of a single monolayer is also maximized, creating optimal conditions for the interference of waves scattered by different monolayers.

The second feature is that there is a fundamentally inherent attenuation of the direct transmittance in the short-wavelength region. For 3-D PCs made of mesoscopic particles the attenuation appears at wavelengths shorter than the position of the photonic pseudogap. It is caused by the energy dissipation due to strong wave scattering on single particles for the wavelengths comparable or shorter than the particles' size. So the single scattering gives rise to the appearance of the transmittance barrier at frequencies higher than the pseudogap. This dissipation cannot be excluded even by perfect ordering of the particles' assembly until their sizes are comparable with the wavelength of the incident light. The existence of this type of loss is the important distinction between light diffraction in 3-D PCs made of mesoscopic particles and Bragg diffraction of x rays in atomic or molecular crystals, where the sizes of the scattering centers are negligible in comparison with the x-ray wavelength and the interatomic spacing.

A related fact is that the complete PBG is hardly achieved for real 3-D PCs composed of particles of an arbitrary shape, but with the particles size comparable to the light wavelength and the interfacial spacing. The cause is strong losses of coherence in the process of light interaction with a single scatterer.

From this point of view it is preferential for some practical applications to use periodical structures with the scatterers smaller than the light wavelength and interfacial spacing. The example of such PC structures for the most attractive visible and infrared ranges is provided by 3-D layer periodic systems of dielectric nanoparticles with interfacial solid subwavelength films.

## ACKNOWLEDGMENTS

This research was supported by the INTAS from grant 01-0642 and partially by the International Scientific and Technical Centre from grant B-276-2.

## REFERENCES

1. C. M. Soukoulis, ed., *Photonic Crystals and Light Localization in the 21st Century* (Kluwer, Dordrecht, The Netherlands, 2001).
2. T. Krauss and T. Baba, eds, "Feature section on photonic crystal structures and applications," *IEEE J. Quantum Electron.* **38**, 724–963 (2002).
3. E. Yablonovitch, "Inhibited spontaneous emission in solid-state physics and electronics," *Phys. Rev. Lett.* **58**, 2059–2062 (1987).
4. S. John, "Strong localization of photons in certain disordered dielectric superlattices," *Phys. Rev. Lett.* **58**, 2486–2489 (1987).
5. K. Ohtaka, "Energy-band of photons and low-energy photon diffraction," *Phys. Rev. B* **19**, 5057–5067 (1979).
6. V. G. Vereshchagin and V. V. Morozov, "New type of cutting filters for the long-wave infrared spectrum region," *Zh. Prikl. Spektrosk.* **49**, 317–320 (1988) (in Russian).
7. J. Martorell and N. M. Lawandy, "Observation of inhibited spontaneous emission in a periodic dielectric structure," *Phys. Rev. Lett.* **65**, 1877–1880 (1990).
8. J. Martorell and N. M. Lawandy, "Distributed feedback oscillation in ordered colloidal suspensions of polystyrene microspheres," *Opt. Commun.* **78**, 169–173 (1990).
9. H. S. Sozuer, J. W. Haus, and R. Inguva, "Photonic bands: convergence problems with the plane-wave method," *Phys. Rev. B* **45**, 13962–13972 (1992).
10. A. Taflove, "Review of the formulation and applications of the finite-difference time-domain method for numerical modeling of electromagnetic-wave interactions with arbitrary structures," *Wave Motion* **10**, 547–582 (1988).
11. P. M. Bell, J. B. Pendry, L. M. Moreno, and A. J. Ward, "A program for calculating photonic band structures and transmission coefficients of complex structures," *Comput. Phys. Commun.* **85**, 306–322 (1995).
12. L.-M. Li and Z.-Q. Zhang, "Multiple-scattering approach to finite-sized photonic band-gap materials," *Phys. Rev. B* **58**, 9587–9590 (1998).
13. G. Tayeb and D. Mayste, "Rigorous theoretical study of finite-size two-dimensional photonic crystals doped by microcavities," *J. Opt. Soc. Am. A* **14**, 3323–3332 (1997).
14. X. D. Wang, X. G. Zhang, Q. L. Yu, and B. N. Harmon, "Multiple-scattering theory for electromagnetic-waves," *Phys. Rev. B* **47**, 4161–4167 (1993).
15. N. Stefanou, V. Yannopoulos, and A. Modinos, "Heterostructures of photonic crystals: frequency bands and transmission coefficients," *Comput. Phys. Commun.* **113**, 49–77 (1998).
16. A. Ishimaru, *Wave Propagation and Scattering in Random Media* (Academic, New York, 1978).
17. V. N. Bogomolov, S. V. Gaponenko, I. N. Germanenko, A. M. Kapitonov, E. P. Petrov, N. V. Gaponenko, A. V. Prokofiev, A. N. Ponyavina, N. I. Silvanovich, and S. M. Samoilovich, "Photonic band gap phenomenon and optical properties of artificial opals," *Phys. Rev. E* **55**, 7619–7625 (1997).
18. A. N. Ponyavina and N. I. Silvanovich, "Interference effects and spectral characteristics of multilayer scattering systems," *Opt. Spectrosc.* **76**, 581–589 (1994).
19. M. Lax, "Multiple scattering of waves. 2. The effective field in dense systems," *Phys. Rev.* **85**, 621–629 (1952).
20. K. M. Hong, "Multiple scattering of electromagnetic waves by a crowded monolayer of spheres: application to migration imaging films," *J. Opt. Soc. Am.* **70**, 821–826 (1980).
21. J. Ziman, *Models of Disorder* (Cambridge U. Press, Cambridge, UK, 1979).
22. S. G. Romanov, N. P. Johnson, A. V. Fokin, V. Y. Butko, H. M. Yates, M. E. Pemble, and C. M. S. Torres, "Enhancement of the photonic gap of opal-based three-dimensional gratings," *Appl. Phys. Lett.* **70**, 2091–2093 (1997).
23. H. Miguez, C. Lopez, F. Meseguer, A. Blanco, L. Vazquez, R. Mayoral, M. Ocana, V. Fornes, and A. Mifsud, "Photonic crystal properties of packed submicrometric SiO<sub>2</sub> spheres," *Appl. Phys. Lett.* **71**, 1148–1150 (1997).
24. J. F. Galisteo-Lopez, E. Palacios-Lidon, E. Castillo-Martinez, and C. Lopez, "Optical study of the pseudogap in thickness and orientation controlled artificial opals," *Phys. Rev. B* **68**, 115109 (2003).
25. S. G. Romanov, A. V. Fokin, and R. M. De La Rue, "Stop-band structure in complementary three-dimensional opal-based photonic crystals," *J. Phys.: Condens. Matter* **11**, 3593–3600 (1999).
26. W. L. Vos, M. Megens, C. M. van Kats, and P. Bosecke, "Transmission and diffraction by photonic colloidal crystals," *J. Phys.: Condens. Matter* **8**, 9503–9507 (1996).
27. C. Bohren and D. Huffman, *Absorption and Scattering of Light by Small Particles* (Wiley, New York, 1983).
28. K. Ohtaka and M. Inoue, "Light-scattering from macroscopic spherical bodies. 2. Reflectivity of light and electromagnetic localized state in a periodic monolayer of dielectric spheres," *Phys. Rev. B* **25**, 689–695 (1982).
29. V. P. Dick, V. A. Loiko, and A. P. Ivanov, "Angular structure of radiation scattered by monolayers of particles: experimental study," *Appl. Opt.* **36**, 4235–4240 (1997).